

Perturbation Study of the Conductance through an Interacting Region Connected to Multi-Mode Leads

Yoshihide TANAKA, Akira OGURI and Hiroumi ISHII

Department of Material Science, Osaka City University, Sumiyoshi-ku, Osaka 558-8585, Japan

(Received August 31, 2001)

We study the effects of electron correlation on transport through an interacting region connected to multi-mode leads based on the perturbation expansion with respect to the inter-electron interaction. At zero temperature the conductance defined in the Kubo formalism can be written in terms of a single-particle Green's function at the Fermi energy, and it can be mapped onto a transmission coefficient of the free quasiparticles described by an effective Hamiltonian. We apply this formulation to a two-dimensional Hubbard model of finite size connected to two noninteracting leads. We calculate the conductance in the electron-hole symmetric case using the order U^2 self-energy. The conductance shows several maximums in the U dependence in some parameter regions of t_y/t_x , where t_x (t_y) is the hopping matrix element in the x - (y -) directions. This is caused by the resonance occurring in some of the subbands, and is related with the U dependence of the eigenvalues of the effective Hamiltonian.

KEYWORDS: conductance, subband structure, electron correlation, perturbation expansion, Hubbard model, two-dimension

§1. Introduction

Low-dimensional electron systems have been one of the current interests in the fields of the condensed matter physics and materials science. For instance, in some of the organic conductors, the electron correlation has been considered to be important to understand the physical properties.¹⁾ The Kondo effect in quantum dots^{2,3,4)} has also been studied intensively from theoretical^{5,6)} and experimental^{7,8,9)} sides. When the average number of the electrons in a quantum dot is odd, the perfect transmission due to the Kondo resonance situated at the Fermi energy occurs at low temperatures. Recently, artificial molecules which are realized by arranging two or more quantum dots have also been studied.^{10,11)} Theoretically, the crossover from the high-temperature Coulomb-blockade to low-temperature Fermi-liquid behaviors of the quantum dots has been studied using advanced numerical methods such as the numerical renormalization group^{12,13)} and quantum Monte Carlo methods.^{14,15,16)}

In a previous work, one of the authors has studied the conductance of small interacting systems

connected to two single-mode leads,^{17,18)} and has calculated the conductance of a Hubbard chain of finite size N using the order U^2 self-energy. The results obtained in the electron-hole symmetric case depend strongly on whether N is even or odd. In the even cases, the conductance decreases with increasing N showing a tendency toward a Mott-Hubbard insulator. On the other hand, in the odd cases the perfect transmission due to the Kondo resonance occurs.¹⁸⁾

The purpose of the present work is to generalize the formulation to the multi-mode systems where the interacting system is connected to noninteracting leads with a number of channels. As in the single-mode case, at $T = 0$ the contributions of the vertex corrections on the dc conductance g vanish. Then the conductance is determined by the value of the single-particle Green's function at the Fermi energy $\omega = 0$, and thus g can be written in terms of the transmission coefficient of the free quasiparticles described by an effective Hamiltonian also in the multi-mode case. We apply the formulation to a two-dimensional Hubbard model of finite size consisting of $N_C = N \times M$ sites, where N and M are the size in the x - and y -direction, respectively. Two noninteracting leads of M channels are attached to this cluster along the x -direction. This system may be considered as a model for two-dimensional materials such as an array of quantum dots and a carbon nanotube. For instance, for $M = 2$ it may also be considered as a model for a ladder system of nanometer size. Since there is no translational symmetry in the systems we are considering, the self-energy has $N_C \times N_C$ matrix elements. We calculate all these elements within the second order perturbation expansion in U in the electron-hole symmetric case, and determine the parameters of the effective Hamiltonian up to terms of order U^2 . The results of the conductance show maximums at finite U for some values of t_y/t_x , where t_x (t_y) is the nearest-neighbor transfer integral in the x -direction (y -direction). This is caused by resonances occurring in some of the subbands. These behaviors can also be understood through the U dependence of the eigenvalues of the effective Hamiltonian. We note that the second-order perturbation theory has been applied by a number of groups to study transport through the single Anderson impurity^{6,19,20,21)} and systems consisting of a number of sites.^{22,23)} Also, the band calculations has been applied to obtain the conductance of nanometer systems.²⁴⁾ Our approach can, in principle, be extended to realistic systems by evaluating the order U^2 self-energy using the orbitals which are obtained with the band calculations.

In §2, we describe the outline of the general formulation and introduce the effective Hamiltonian. In §3, we apply the method to a two-dimensional Hubbard model, and present the results of the conductance. Summary is given in §4. In Appendix, we provide the derivation of the expressions of the conductance and the total charge displacement.

§2. Formulation

In this section, we give the outline of a general formulation of the conductance through interacting systems connected to Fermi-liquid reservoirs with a number of channels. Our formulation is applicable for various systems which have the time reversal symmetry, i.e., eqs. (2.9) and (2.11)

hold for a wide range of the systems described by the Hamiltonian eq. (2.1). We provide the details of the derivations in Appendix, and demonstrate the application to a Hubbard model in the next section.

We start with a system which consists of three regions as illustrated in Fig. 1; a finite interacting region (C) situated in the middle, and two noninteracting reservoirs on the left (L) and right (R). The central region contains N_C resonant levels, and the inter-electron interaction $U_{j_4 j_3; j_2 j_1}$ is switched on in the central region. Each of the two reservoirs is infinitely large and has a continuous energy spectrum. The central region and two reservoirs are connected by M_L and M_R channels which are described by the mixing matrix elements $v_{L,m}$ and $v_{R,m}$, respectively. The complete Hamiltonian is given by

$$\mathcal{H} = \mathcal{H}_L + \mathcal{H}_R + \mathcal{H}_C^0 + \mathcal{H}_C^{\text{int}} + \mathcal{H}_{\text{mix}}, \quad (2.1)$$

$$\mathcal{H}_L = \sum_{ij \in L} \sum_{\sigma} \left(-t_{ij}^L - \mu \delta_{ij} \right) c_{i\sigma}^{\dagger} c_{j\sigma}, \quad (2.2)$$

$$\mathcal{H}_R = \sum_{ij \in R} \sum_{\sigma} \left(-t_{ij}^R - \mu \delta_{ij} \right) c_{i\sigma}^{\dagger} c_{j\sigma}, \quad (2.3)$$

$$\mathcal{H}_C^0 = \sum_{ij \in C} \sum_{\sigma} \left(-t_{ij}^C - \mu \delta_{ij} \right) c_{i\sigma}^{\dagger} c_{j\sigma}, \quad (2.4)$$

$$\mathcal{H}_C^{\text{int}} = \frac{1}{2} \sum_{\{j\} \in C} \sum_{\sigma\sigma'} U_{j_4 j_3; j_2 j_1} c_{j_4\sigma}^{\dagger} c_{j_3\sigma'}^{\dagger} c_{j_2\sigma'} c_{j_1\sigma}, \quad (2.5)$$

$$\begin{aligned} \mathcal{H}_{\text{mix}} = & - \sum_{m=1}^{M_L} \sum_{\sigma} v_{L,m} \left(c_{\mathcal{I}_m\sigma}^{\dagger} c_{\mathcal{L}_m\sigma} + c_{\mathcal{L}_m\sigma}^{\dagger} c_{\mathcal{I}_m\sigma} \right) \\ & - \sum_{m=1}^{M_R} \sum_{\sigma} v_{R,m} \left(c_{\mathcal{R}_m\sigma}^{\dagger} c_{\mathcal{N}_m\sigma} + c_{\mathcal{N}_m\sigma}^{\dagger} c_{\mathcal{R}_m\sigma} \right). \end{aligned} \quad (2.6)$$

Here $c_{j\sigma}^{\dagger}$ ($c_{j\sigma}$) creates (destroys) an electron with spin σ at site j , and μ is the chemical potential. t_{ij}^L , t_{ij}^R , and t_{ij}^C are the intra-region hopping matrix elements in each of the regions L, R, and C, respectively. The labels $1, 2, \dots, N_C$ are assigned to the sites in the central region. In eq. (2.6), \mathcal{I}_m (\mathcal{L}_m) is the label assigned to the m -th site at the sample side (lead side) of the interface on the left. \mathcal{N}_m (\mathcal{R}_m) is the label assigned to the m -th site at the sample side (lead side) of the interface on the right. Note that the number of the channels is less than the number of the interacting sites, i.e., $M_L \leq N_C$ and $M_R \leq N_C$. For instance, in the case of $M_L = M_R = N_C$, all the sites in the central region are connected to both of the reservoirs, i.e., $\mathcal{I}_m = \mathcal{N}_m$ for $m = 1, 2, \dots, N_C$. We assume that all the hopping matrix elements are real, and the interaction has the time reversal symmetry: $U_{43;21}$ is real and $U_{43;21} = U_{34;12} = U_{12;34} = U_{42;31} = U_{13;24}$. We will be using units $\hbar = 1$ unless otherwise noted.

The single-particle Green's function is defined by

$$G_{jj'}(i\varepsilon_n) = - \int_0^{\beta} d\tau \left\langle T_{\tau} c_{j\sigma}(\tau) c_{j'\sigma}^{\dagger}(0) \right\rangle e^{i\varepsilon_n \tau}. \quad (2.7)$$

Here $\beta = 1/T$, $\varepsilon_n = (2n + 1)\pi/\beta$, $c_{j\sigma}(\tau) = e^{\tau\mathcal{H}}c_{j\sigma}e^{-\tau\mathcal{H}}$, and $\langle \dots \rangle$ denotes the thermal average $\text{Tr} [e^{-\beta\mathcal{H}} \dots] / \text{Tr} e^{-\beta\mathcal{H}}$. The spin index has been omitted from the left-hand side of eq. (2.7) assuming the expectation value to be independent of whether spin is up or down. Since the interaction is switched on only for the electrons in the central region, the Dyson equation can be written as

$$G_{ij}(z) = G_{ij}^0(z) + \sum_{i'j' \in \mathcal{C}} G_{ii'}^0(z) \Sigma_{i'j'}(z) G_{j'j}(z). \quad (2.8)$$

Here $G_{ij}^0(z)$ is the unperturbed Green's function corresponding to the noninteracting Hamiltonian $\mathcal{H}^0 \equiv \mathcal{H}_L + \mathcal{H}_R + \mathcal{H}_C^0 + \mathcal{H}_{\text{mix}}$. The summations with respect to i' and j' run over the sites in the central region, and $\Sigma_{i'j'}(z)$ is the self-energy due to the interaction $\mathcal{H}_C^{\text{int}}$. Because of the time reversal symmetry of \mathcal{H} , these functions are symmetric against the interchange of the site indices: $G_{ij}(z) = G_{ji}(z)$ and $\Sigma_{ij}(z) = \Sigma_{ji}(z)$. Note that at $T = 0$ the single-particle excitation at the Fermi energy $z = i0^+$ does not decay, i.e., $\text{Im} \Sigma_{ij}^+(0) = 0$.³³⁾ In what follows, we will treat z as a complex variable, and use the symbol $+$ ($-$) in the superscript as a label for the retarded (advanced) function: $\Sigma_{ij}^\pm(\varepsilon) \equiv \Sigma_{ij}(\varepsilon \pm i0^+)$.

As in the single-mode case, the dc conductance at $T = 0$ can be expressed in terms of the single-particle Green's function at $\omega = 0$ [see Appendix A];

$$g = \frac{2e^2}{h} \text{Tr} \left[4 \mathbf{\Gamma}_R(0) \mathbf{G}_{\mathcal{N}\mathcal{I}}^+(0) \mathbf{\Gamma}_L(0) \mathbf{G}_{\mathcal{I}\mathcal{N}}^-(0) \right]. \quad (2.9)$$

Here $\mathbf{\Gamma}_L(\omega)$ and $\mathbf{\Gamma}_R(\omega)$ are $M_L \times M_L$ and $M_R \times M_R$ matrices, respectively. These two matrices are caused by the coupling with the left (L) and right (R) leads, and the elements are given by $\Gamma_{\alpha;mm'}(\omega) = -\text{Im} [v_{\alpha,m} F_{\alpha,mm'}^+(\omega) v_{\alpha,m'}]$ with $F_{\alpha,mm'}(z)$ being the Green's functions at the interface of the isolated lead ($\alpha = L, R$). In eq. (2.9), $\mathbf{G}_{\mathcal{N}\mathcal{I}}^+$ and $\mathbf{G}_{\mathcal{I}\mathcal{N}}^-$ are $M_R \times M_L$ and $M_L \times M_R$ matrices the elements of which are given by $G_{\mathcal{N}_i\mathcal{I}_m}^+$ and $G_{\mathcal{I}_i\mathcal{N}_m}^-$, respectively.

Another quantity which can be related to the scattering coefficients is the displacement of the total charge defined by^{33,34)}

$$\begin{aligned} \Delta N_{\text{tot}} &= \sum_{i \in \mathcal{C}} \sum_{\sigma} \langle c_{i\sigma}^\dagger c_{i\sigma} \rangle \\ &+ \sum_{i \in \mathcal{L}} \sum_{\sigma} \left[\langle c_{i\sigma}^\dagger c_{i\sigma} \rangle - \langle c_{i\sigma}^\dagger c_{i\sigma} \rangle_{\mathcal{L}} \right] \\ &+ \sum_{i \in \mathcal{R}} \sum_{\sigma} \left[\langle c_{i\sigma}^\dagger c_{i\sigma} \rangle - \langle c_{i\sigma}^\dagger c_{i\sigma} \rangle_{\mathcal{R}} \right]. \end{aligned} \quad (2.10)$$

Here $\langle \dots \rangle_{\mathcal{L}}$ and $\langle \dots \rangle_{\mathcal{R}}$ denote the ground-state average of isolated leads described by \mathcal{H}_L and \mathcal{H}_R , respectively. At $T = 0$, following the derivation of the Friedel sum rule by Langer and Ambegaokar,³³⁾ ΔN_{tot} can be written in terms of a $(M_L + M_R) \times (M_L + M_R)$ matrix \mathbf{S} ,

$$\Delta N_{\text{tot}} = \frac{1}{\pi i} \log[\det \mathbf{S}], \quad (2.11)$$

$$\mathbf{S} = \mathbf{1} - 2i \begin{bmatrix} \boldsymbol{\Gamma}_L(0) & \mathbf{o} \\ \mathbf{o} & \boldsymbol{\Gamma}_R(0) \end{bmatrix} \begin{bmatrix} \mathbf{G}_{\mathcal{I}\mathcal{I}}^+(0) & \mathbf{G}_{\mathcal{I}\mathcal{N}}^+(0) \\ \mathbf{G}_{\mathcal{N}\mathcal{I}}^+(0) & \mathbf{G}_{\mathcal{N}\mathcal{N}}^+(0) \end{bmatrix}. \quad (2.12)$$

Here $\mathbf{G}_{\mathcal{I}\mathcal{I}}^+$ and $\mathbf{G}_{\mathcal{N}\mathcal{N}}^+$ are $M_L \times M_L$ and $M_R \times M_R$ matrices, and the elements are given by $G_{\mathcal{I}_l\mathcal{I}_m}^+$ and $G_{\mathcal{N}_l\mathcal{N}_m}^+$, respectively. The outline of the Friedel sum rule in the single-mode case is given in Appendix B. The extension to multi-mode case eq. (2.11) is straightforward because in the case of the Friedel sum rule we do not have to take into account the contributions vertex corrections. For convenience, in eq. (2.12) we have assumed that there is no common element in the sets \mathcal{I} and \mathcal{N} . This is not an important assumption, and the expression without the assumption can be obtained in the similar way. Note that eq. (2.11) is also written in terms of the Green's function at $T = 0$ and $\omega = 0$. Thus, due to the property $\text{Im} \Sigma_{ij}^+(0) = 0$, the values of g and ΔN_{tot} at $T = 0$ can be expressed in terms of the transmission and reflection coefficients defined with respect to a one-particle Hamiltonian¹⁸⁾

$$\tilde{\mathcal{H}}_{\text{qp}} = \mathcal{H}_L + \mathcal{H}_R + \mathcal{H}_C^{\text{eff}} + \mathcal{H}_{\text{mix}}. \quad (2.13)$$

Here $\mathcal{H}_C^{\text{eff}} = \sum_{ij \in C, \sigma} \left(-\tilde{t}_{ij}^C - \mu \delta_{ij} \right) c_{i\sigma}^\dagger c_{j\sigma}$ with $-\tilde{t}_{ij}^C = -t_{ij}^C + \text{Re} \Sigma_{ij}^+(0)$. This effective Hamiltonian describes free quasiparticles of the local Fermi-liquid. As shown in the next section, the eigenvalues of the partial Hamiltonian $\mathcal{H}_C^{\text{eff}}$ have important information about the ground-state properties.

§3. Application to a Two-dimensional Hubbard Model

In this section, we apply the formulation to a two-dimensional Hubbard model connected to reservoirs and calculate the conductance using the order U^2 self-energy in the electron-hole symmetric case.

3.1 Model

The schematic picture of the model is illustrated in Fig. 2. The system size in the y -direction, M , is finite. In the x -direction, the central region consists of N columns, and two noninteracting leads are connected at $x = 1$ and $x = N$. Thus, the total number of the interacting sites is $N_C = N \times M$. The parameters of the Hamiltonian eq. (2.1) are specified as follows. The mixing matrix element is assumed to be uniform in the y -direction: $v_{L,m} = v_L$ and $v_{R,m} = v_R$ for $m = 1, 2, \dots, M$. We assume that the off diagonal part of t_{ij}^C describes the nearest-neighbor hopping; t_x and t_y in the x - and y -directions, respectively. Along the y -direction, we use the periodic boundary condition. Furthermore, we assume $U_{j_4 j_3; j_2 j_1}$ to be an onsite repulsion U , and concentrate on the electron-hole symmetric case taking the parameters to be $\mu = 0$ and $\epsilon_d + U/2 = 0$, where ϵ_d is the onsite energy of the interacting sites $-t_{ii}^C = \epsilon_d$. Then the Dyson equation can be written in a $N_C \times N_C$ matrix

form: $\{\widehat{\mathcal{G}}(z)\}^{-1} = \{\widehat{\mathcal{G}}^0(z)\}^{-1} - \widehat{\Sigma}(z)$ with

$$\{\widehat{\mathcal{G}}^0(z)\}^{-1} = z \widehat{\mathbf{1}} - \widehat{\mathcal{H}}_C^0 - \widehat{\mathcal{V}}_{\text{mix}}(z). \quad (3.1)$$

Here $\widehat{\mathbf{1}}$ is the $N_C \times N_C$ unit matrix, and the matrices can be written in the partitioned forms;

$$\widehat{\mathcal{H}}_C^0 = \begin{bmatrix} \mathbf{h}_y^0 & -t_x \mathbf{1} & & \mathbf{0} \\ -t_x \mathbf{1} & \ddots & \ddots & \\ & \ddots & \ddots & -t_x \mathbf{1} \\ \mathbf{0} & & -t_x \mathbf{1} & \mathbf{h}_y^0 \end{bmatrix}, \quad (3.2)$$

$$\widehat{\mathcal{V}}_{\text{mix}}(z) = \begin{bmatrix} v_L^2 \mathbf{F}_L(z) & & & \\ & \mathbf{0} & & \\ & & & v_R^2 \mathbf{F}_R(z) \end{bmatrix}, \quad (3.3)$$

$$\widehat{\Sigma}(z) = \begin{bmatrix} \Sigma_{11}(z) & \Sigma_{12}(z) & \dots & \Sigma_{1N}(z) \\ \Sigma_{21}(z) & \ddots & \ddots & \vdots \\ \vdots & \ddots & \ddots & \vdots \\ \Sigma_{N1}(z) & \dots & \dots & \Sigma_{NN}(z) \end{bmatrix}, \quad (3.4)$$

where $\mathbf{1}$ is the $M \times M$ unit matrix, and \mathbf{h}_y^0 is the $M \times M$ hopping matrix in the y -direction;

$$\mathbf{h}_y^0 = \begin{bmatrix} 0 & -t_y & & & -t_y \\ -t_y & 0 & -t_y & & \mathbf{0} \\ & -t_y & 0 & \ddots & \\ & & \ddots & \ddots & \ddots \\ \mathbf{0} & & & \ddots & \ddots & -t_y \\ -t_y & & & & -t_y & 0 \end{bmatrix}. \quad (3.5)$$

We note that the Hartree-Fock term of the self-energy is already included in the unperturbed Green's function $\widehat{\mathcal{G}}^0(z)$ defined by eq. (3.1). Therefore, $\widehat{\Sigma}(z)$ is the self-energy correction beyond the mean-field theory, which is described by the many-body perturbation theory with respect to $\mathcal{H}_C^{\text{int}} = U \sum_{i=1}^{N_C} [n_{i\uparrow} n_{i\downarrow} - (n_{i\uparrow} + n_{i\downarrow})/2]$ where $n_{i\sigma} = c_{i\sigma}^\dagger c_{i\sigma}$. We note that the mixing with the noninteracting leads is included in the unperturbed Hamiltonian, and thus $\widehat{\Sigma}(z)$ depends on v_L and v_R through $\widehat{\mathcal{G}}^0(z)$. In eq. (3.4) the partitioned element $\Sigma_{ll'}(z)$ is a $M \times M$ matrix the (m, m') element of which corresponds to the self-energy correction between the sites located at $\mathbf{r} = (l, m)$ and $\mathbf{r}' = (l', m')$, where l and m correspond to the x and y coordinates, respectively. The local Green's functions at the interfaces of the isolated leads, $\mathbf{F}_L(z)$ and $\mathbf{F}_R(z)$ in eq. (3.3), depend on the excitation spectrum of the leads, i.e., \mathcal{H}_L and \mathcal{H}_R . We concentrate on the case $\mathbf{F}_L = \mathbf{F}_R$ ($\equiv \mathbf{F}$) assuming the same excitation spectrum for the left and right leads. Then the matrices of the level width are given by $\Gamma_L(\omega) = -v_L^2 \text{Im} \mathbf{F}(\omega + i0^+)$ and $\Gamma_R(\omega) = -v_R^2 \text{Im} \mathbf{F}(\omega + i0^+)$. For

the function $\mathbf{F}(z)$, we consider two types models: I) semi-infinite tight-binding leads, and II) leads of a constant density of states. A schematic picture of the type I lead is illustrated in Fig. 3: the hopping matrix element is given by the nearest neighbor one, t_x and t_y , as that in the central region. Therefore the Green's function for the type I lead \mathbf{F}^I satisfies a $M \times M$ matrix equation $\mathbf{F}^I(z) = [z\mathbf{1} - \mathbf{h}_y^0 - t_x^2 \mathbf{F}^I(z)]^{-1}$. In the case of the type II leads, we assume that the local density of states at the interfaces ρ is a constant and the bandwidth is infinity. Then the corresponding retarded Green's function becomes pure imaginary independent of the frequency ω . Specifically, we consider a simple diagonal matrix of the form $\mathbf{F}^{II}(\omega + i0^+) = -i\pi\rho\mathbf{1}$. Thus for the type II leads, the effects of the mixing are parametrized by the constant $\Gamma_\alpha = \pi\rho v_\alpha^2$ for $\alpha = L$ and R .

The subband structure of the system is determined by the eigenstates of eq. (3.5): $\mathbf{h}_y^0 \boldsymbol{\chi}_n = \epsilon_n \boldsymbol{\chi}_n$ for $n = 1, 2, \dots, M$. Due to the translational symmetry in the y -direction, the self-energy $\boldsymbol{\Sigma}_{ll'}$ (z) and the $M \times M$ matrix Green's function $\mathbf{G}_{ll'}$ (z), which are the (l, l') partitioned element of $\widehat{\mathcal{G}}(z)$, can be diagonalized using the eigenstates;

$$\boldsymbol{\Sigma}_{ll'}(z) = \sum_{n=1}^M \boldsymbol{\chi}_n \Sigma_{ll'}^{(n)}(z) \boldsymbol{\chi}_n^\dagger, \quad (3.6)$$

$$\mathbf{G}_{ll'}(z) = \sum_{n=1}^M \boldsymbol{\chi}_n G_{ll'}^{(n)}(z) \boldsymbol{\chi}_n^\dagger. \quad (3.7)$$

Therefore, the conductance eq. (2.9) can be decomposed into the sum of the contributions of the subbands:

$$g = \frac{2e^2}{h} \sum_{n=1}^M 4\Gamma_R^{(n)}(0) G_{N1}^{(n)+}(0) \Gamma_L^{(n)}(0) G_{1N}^{(n)-}(0). \quad (3.8)$$

Here $\Gamma_\alpha^{(n)}(0)$ is defined by $\boldsymbol{\Gamma}_\alpha(z) = \sum_{n=1}^M \boldsymbol{\chi}_n \Gamma_\alpha^{(n)}(z) \boldsymbol{\chi}_n^\dagger$ for $\alpha = L, R$. Similarly, the Friedel sum rule eq. (2.11) can be rewritten as

$$\Delta N_{\text{tot}} = \frac{2}{\pi} \sum_{n=1}^M \frac{1}{2i} \log [\det \mathbf{S}^{(n)}], \quad (3.9)$$

$$\mathbf{S}^{(n)} = \begin{bmatrix} 1 & 0 \\ 0 & 1 \end{bmatrix} - 2i \begin{bmatrix} \Gamma_L^{(n)}(0) & 0 \\ 0 & \Gamma_R^{(n)}(0) \end{bmatrix} \begin{bmatrix} G_{11}^{(n)+}(0) & G_{1N}^{(n)+}(0) \\ G_{N1}^{(n)+}(0) & G_{NN}^{(n)+}(0) \end{bmatrix}. \quad (3.10)$$

Here $\delta^{(n)} \equiv 1/(2i) \log [\det \mathbf{S}^{(n)}]$ corresponds to the phase shift of the n -th subband, and the charge displacement in each subband is given by $\Delta N_{\text{tot}}^{(n)} = 2\delta^{(n)}/\pi$. As mentioned, at $T = 0$ the conductance is determined by the value of the Green's function at $\omega = 0$, and $\text{Im} \widehat{\boldsymbol{\Sigma}}^+(0) = \widehat{\mathbf{o}}$ due to the Fermi-liquid property. Thus the effective Hamiltonian $\widehat{\mathcal{H}}_C^{\text{eff}} = \widehat{\mathcal{H}}_C^0 + \text{Re} \widehat{\boldsymbol{\Sigma}}^+(0)$, which was introduced in the previous section, can be used to calculate the conductance and the displacement

of the total charge.¹⁸⁾ We now consider the $M \times M$ matrix $\mathcal{H}_{C;l'l'}^{\text{eff}}$, which is the partitioned element of $\widehat{\mathcal{H}}_C^{\text{eff}}$. The matrix $\mathcal{H}_{C;l'l'}^{\text{eff}}$ can also be diagonalized as

$$\mathcal{H}_{C;l'l'}^{\text{eff}} = - \sum_{n=1}^M \chi_n \tilde{t}_{l'l'}^{(n)} \chi_n^\dagger, \quad (3.11)$$

$$-\tilde{t}_{l'l'}^{(n)} = \epsilon_n \delta_{l'l'} - t_x [\delta_{l,l'+1} + \delta_{l+1,l'}] + \text{Re} \Sigma_{l'l'}^{(n)+}(0), \quad (3.12)$$

where $1 \leq l, l' \leq N$. Thus each of the modes can be mapped onto a tight-binding model in one-dimension with the renormalized hopping matrix element $\tilde{t}_{l'l'}^{(n)}$. As it will be seen later, the behavior of eigenvalues of the $N \times N$ effective Hamiltonian defined by $\widetilde{\mathcal{H}}_C^{(n)} = \{-\tilde{t}_{l'l'}^{(n)}\}$ is related to the transport properties.

We calculate the conductance using the perturbation expansion with respect to U . In the electron-hole symmetric case, the order U^2 self-energy can be described by the diagram shown in Fig. 4;

$$\begin{aligned} \Sigma_{jj'}^+(0) = & \\ & -U^2 \int_{-\infty}^{\infty} \int_{-\infty}^{\infty} \frac{d\varepsilon d\varepsilon'}{(2\pi)^2} G_{jj'}^0(i\varepsilon) G_{jj'}^0(i\varepsilon') G_{j'j}^0(i\varepsilon + i\varepsilon'), \end{aligned} \quad (3.13)$$

where $1 \leq j, j' \leq N_C$. The explicit form of the unperturbed Green's function $G_{jj'}^0(i\varepsilon)$ can be obtained by taking the inverse of eq. (3.1). Since \mathcal{H}_{mix} is included in the unperturbed part, $G_{jj'}^0$ and $\Sigma_{jj'}^+$ depend on the mixing matrix elements v_L and v_R . Note that the retarded function at $\omega = 0$ can be obtained from the Matsubara function, i.e., $\Sigma_{jj'}^+(0) = \Sigma_{jj'}(i\varepsilon)|_{\varepsilon \rightarrow 0^+}$. The imaginary part of eq. (3.13) vanishes, i.e., $\text{Im} \Sigma_{jj'}^+(0) = 0$ owing to the Fermi-liquid property. Furthermore, due to the electron-hole symmetry, $\text{Re} \Sigma_{jj'}^+(0) = 0$ if j and j' belong to the same sublattice. We calculate all the nonzero elements of $\text{Re} \Sigma_{jj'}^+(0)$ carrying out the integrations in eq. (3.13) numerically. Then the full Green's function $\mathbf{G}_{N1}^+(0)$ is evaluated substituting the order U^2 self-energy into the Dyson equation. In what follows we will assume the inversion symmetry $v_L = v_R$ ($\equiv v$), and take the parameter to be $v/t_x = 0.9$ in the case of the type I leads. We have actually done some calculations also for $v/t_x = 0.7$, but the results are similar to those for $v/t_x = 0.9$ qualitatively. Correspondingly, in the case of the type II leads we set $\Gamma_L = \Gamma_R$ ($\equiv \Gamma$) and take the value to be $\Gamma/t_x = 0.75$. We will mainly discuss the results obtained for the leads of the width $M = 4$.

3.2 Noninteracting systems

We now discuss some properties in the noninteracting case in order to show the situations we are considering clear. Fig. 5 shows the conductance $g_{\text{1d}}^0(E_F)$ for noninteracting electrons in the one-dimensional systems connected to the leads of the type I (solid line) and II (dashed line). In this figure, E_F is the Fermi-energy, and the size of the central region is taken to be $N = 4$. The coupling

with the leads are taken to be $v/t_x = 0.9$ for the type I leads, and $\Gamma/t_x = 0.75$ for the type II leads. There are $N (= 4)$ peaks of the resonance, and the peaks become sharp if the mixing matrix element v/t_x or Γ/t_x decreases. In two dimensional lattice with the periodic boundary condition in the y -direction, the conductance for noninteracting electrons is given by $g_{2d}^0 = \sum_{n=1}^M g_{1d}^0(\epsilon_n)$ in the electron-hole symmetric case. For instance, in the case of $M = 4$, the eigenvalues ϵ_n are given by $\epsilon_1 = -\epsilon_4 = 2t_y$, and $\epsilon_2 = \epsilon_3 = 0$. Therefore, when t_y decreases, the conductance shows peaks corresponding to the resonance occurring in the one-dimensional system $g_{1d}^0(\epsilon_n)$.

As an example of the the subband structure in the case of the type I leads, we show the dispersion relation of an ideal system $E_{nk_x} = -2t_x \cos k_x + \epsilon_n$ in Fig. 6. Here the size along the y -direction is taken to be $M = 4$, and the hopping matrix elements are taken to be $t_y/t_x = 1.0$ (solid line) and $t_y/t_x = 0.5$ (dashed line). In the case of $t_y/t_x = 1.0$ the highest and lowest subbands, i.e., modes 1 and 4, do not contribute to the conductance because the Fermi energy is situated at the band edge of the subbands. These two subband become conducting for $0.0 < t_y/t_x < 1.0$. We note that the modes 2 and 3 are degenerate and several curves are overlaps on the line corresponding to $-2t_x \cos k_x$ in Fig. 6.

3.3 Hubbard model connected to the type I leads

In this subsection, we discuss the results for the Hubbard model connected to the type I leads. The conductance g for the isotropic hopping $t_y/t_x = 1.0$ is shown as a function of U in Fig. 7, where the size of the interacting region in the y -direction is $M = 4$ and that in the x -direction is $N = 4, 6, 8$, and 10. The conductance decreases with increasing U . The N dependence is similar to that in the one-dimensional case, i.e., g decreases monotonically with increasing N showing a tendency toward the Mott-Hubbard insulator.¹⁸⁾ As mentioned in the above, the modes 1 and 4 are not conducting in the case of $t_y/t_x = 1.0$, and the conductance is determined by the contributions of the modes 2 and 3. This situation is changed in the anisotropic cases $t_y/t_x < 1.0$.

In Fig. 8, the conductance is plotted for several values of t_y/t_x , where the size of the interacting region is taken to be $N = 4$ and $M = 4$. There is a broad peak at finite U for $0.65 \lesssim t_y/t_x \lesssim 0.75$. This shows that there are parameter regions where the total conductance increases with U even in the half-filled case. To clarify this behavior, in Fig. 9 the contributions of each of the conducting modes are plotted separately taking t_y/t_x to be 0.7. The resonant tunneling occurs in the modes 1 and 4 at $U/(2\pi t_x) \simeq 3.3$, while the contributions of the modes 2 and 3 decreases monotonically with increasing U . Note that the pair of the subbands whose wavenumber in the y -direction are k_y and $-k_y$ give the same contributions to the conductance. Furthermore in the electric-hole symmetric case, the contributions of the subbands whose eigenvalues are ϵ_n and $-\epsilon_n$ are the same. The occurrence of the resonant tunneling is linked with the behavior of the eigenvalues of effective Hamiltonian which is defined in terms of the renormalized hopping matrix element $-\tilde{t}_{ll'}^{(n)}$ given by eq. (3.12). In Fig. 10, the eigenvalue of the $N \times N$ matrix $\tilde{\mathcal{H}}_C^{(n)}$ is plotted as a function of U for the

mode 1 (solid line), where $t_y/t_x = 0.7$, $N = 4$ and $M = 4$. The second lowest eigenvalue crosses the Fermi energy at $U/(2\pi t_x) \simeq 4.6$. This corresponds to the peak seen at $U/(2\pi t_x) \simeq 3.3$ in Fig. 9, although the values of U do not coincide. This difference is mainly due to the contribution of the real part of the mixing term eq. (3.3): $\text{Re}\hat{\mathcal{V}}_{\text{mix}}^+(0)$ causes the energy shift, and the position of the resonance corresponding to the second eigenvalue moves toward the low-energy side. While the transmission probability is defined with respect to the effective Hamiltonian of the whole system $\tilde{\mathcal{H}}_{\text{qp}}$ in eq. (2.13), the eigenvalues of the partial Hamiltonian $\tilde{\mathcal{H}}_C^{(n)}$ are useful to investigate the behaviors of the conductance. Note that $\tilde{t}_{ll'}^{(n)}$ depends on the mixing matrix elements v_L and v_R because the unperturbed Green's functions used to calculate the self-energy eq. (3.13) are defined with respect to the whole system. In Fig. 10, the eigenvalues for the modes 2 and 3 are also plotted (dashed lines). In the present case, the eigenvalues of the modes 2 and 3 are the same, and the eigenvalues of the modes 1 and 4 are symmetric with respect to the Fermi energy $\omega = 0$. The energy gap between the second and third eigenvalues of the mode 2 (or 3) becomes large with increasing U , and it seems to show the tendency toward the Mott-Hubbard insulator.

We have also examined the conductance in the case of $M = 6$, where the subbands are classified into two groups; $\epsilon_1 = -\epsilon_6 = 2t_y$ and $\epsilon_2 = \epsilon_3 = -\epsilon_4 = -\epsilon_5 = t_y$. In Fig. 11, the total conductance (solid line) and the contributions of the two groups of subbands (dashed line) are shown for $t_y/t_x = 0.65$, where the size of the interacting region is taken to be $N = 6$ and $M = 6$. The total conductance show two bump like behaviors at $U/(2\pi t_x) \simeq 1.5$ and 5.1 , which correspond to the resonance occurring in each group of the subbands. The resonance occurs at different values of U for the different groups of the subbands. This seems to show a general tendency that the resonance does not occur simultaneously in the different groups of the subbands. Thus, when the resonance occurs at one group, the remaining $M - 2$ or $M - 4$ subbands behave monotonically. Therefore the presence of the visible maximum in the U dependence of the total conductance is expected only for small M where the contributions of the resonating subbands are comparable to the those of the remaining subbands.

The number of the eigenvalues which cross the Fermi energy is expected to increase with the size in the x -direction N . To clarify this feature, we calculate the conductance for $N = 10$ keeping the width $M = 4$ unchanged. The results are shown in Fig. 12 for several values of t_y/t_x . In each of the cases, at least one peak is visible at finite U . Specifically in the case of $t_y/t_x = 0.5$, a shoulder like structure is seen at $U/2\pi t_x \simeq 0.5$ in addition to the peak at $U/2\pi t_x \simeq 3.8$. To see this behavior precisely, the contributions of each of the subbands are plotted in Fig. 13. Two resonant peaks are seen at $U/(2\pi t_x) \simeq 0.5$ and 3.8 in the modes 1 and 4. The U dependence of the eigenvalues of $\tilde{\mathcal{H}}_C^{(n)}$ for $n = 1$ (mode 1) is shown in Fig. 14. The 4th and 5th lowest eigenvalues cross the Fermi energy at $U/(2\pi t_x) \simeq 0.7$ and 4.1 , respectively. These correspond to the two resonant peaks seen in Fig. 13 as in the case of $N = 4$. The energy shift caused by the mixing with the leads seems to decrease

with increasing N .

3.4 Hubbard model connected to the type II leads

We next discuss the conductance of the Hubbard model connected to the type II leads. In this lead, the local density of states at the interface of the lead is a constant and the bandwidth is infinity. Then $\widehat{\mathcal{V}}_{\text{mix}}^+(\omega)$ becomes pure imaginary and independent of ω , i.e., $\text{Re } \widehat{\mathcal{V}}_{\text{mix}}^+(\omega) \equiv 0$ and $\partial \widehat{\mathcal{V}}_{\text{mix}}^+(\omega)/\partial \omega \equiv 0$. Therefore the energy shift caused by the mixing with the leads is expected to be small compared to that in the case of the leads I. In Fig. 15 (a), the conductance in the case of $t_y/t_x = 0.6$ and 0.78 is shown as a function of U , where the size of the interacting region is chosen to be $N = 4$ and $M = 4$. There is a resonance peak at finite U in each line; at $U/(2\pi t_x) \simeq 4.3$ for $t_y/t_x = 0.6$ and $U/(2\pi t_x) \simeq 0.6$ for $t_y/t_x = 0.78$. The contributions of each of the subbands are plotted separately in Fig. 15 (b). The peak seen in the total conductance is due to the resonance tunneling in the modes 1 and 4. Qualitatively, these results are similar to those of the type I leads. In Fig. 16, the eigenvalues of the effective Hamiltonian $\widetilde{\mathcal{H}}_C^{(n)}$ for $n = 1$ (mode 1) are plotted for (a) $t_y/t_x = 0.6$ and (b) $t_y/t_x = 0.78$. The second lowest eigenvalue for $t_y/t_x = 0.6$ becomes zero at $U/(2\pi t_x) \simeq 4.1$. This is close to the position of the resonance peak seen in Fig. 15 (b). The lowest eigenvalue for $t_y/t_x = 0.78$ does not cross the Fermi energy for any values of U , although it is nearly zero for small U . Nevertheless, this eigenstate corresponds to the resonance peak seen at $U/(2\pi t_x) \simeq 0.6$ in Fig. 15 (b). This is because the lowest eigenvalue is shifted slightly up due to the mixing, and it becomes to cross the Fermi energy.

We next discuss the phase shift $\delta^{(n)}$. As mentioned, the charge displacement of the n -th subband can be deduced from the phase shift using the Friedel sum rule $\Delta N_{\text{tot}}^{(n)} = 2\delta^{(n)}/\pi$, where the factor 2 corresponds to the spin degeneracy. Specifically, in the case of the type II leads, the compensation theorem holds.²⁵⁾ Then the second and the third term in the right-hand of eq. (2.10) vanish because $\widehat{\mathcal{V}}_{\text{mix}}^+(\omega)$ is independent of ω (see also Appendix B). Thus the number of electrons in the type II leads is unchanged when the leads are connected to the interacting region, and the left-hand side of eq. (3.9), ΔN_{tot} , becomes equal to the number of electrons in the interacting region $\sum_{i \in C, \sigma} \langle c_{i\sigma}^\dagger c_{i\sigma} \rangle$. In Fig. 17, the phase shift $\delta^{(n)}/\pi$ is plotted as a function of U for the modes 1 and 4, where the parameters are taken to be $N = 4$, $M = 4$, and $t_y/t_x = 0.78$. Here the principal value of the phase shift is determined in the limit of $U \rightarrow 0$ by comparing with the charge displacement obtained independently. Reflecting the resonance seen in Fig. 15 (b), $\delta^{(n)}$ for the mode 1 starts to increase rapidly at $U/(2\pi t_x) \simeq 0.6$. Correspondingly in the mode 4, which is the lowest subband in this case, the phase shift $\delta^{(4)}$ decreases. These behaviors show how the filling of the subband changes when the resonance peak crosses the Fermi energy. In Fig. 17, the sum of the two phase shifts is a constant, i.e., $2\delta^{(1)}/\pi + 2\delta^{(4)}/\pi = 2N$ with $N = 4$. The phase shifts for the modes 2 and 3 are the same, and it is a constant independent of U , i.e., $2\delta^{(n)}/\pi = N$ for $n = 2$ and 3 with $N = 4$. This means that these two subbands are half filled. Note that the total charge displacement is given by

$\Delta N_{\text{tot}} = M \times N$ in the electron-hole symmetric case.

3.5 Remarks

The results presented in this section are obtained using the order U^2 self-energy given by eq. (3.13). Therefore, the results plotted for rather large values of U may not be sufficient in quantitative sense. Nevertheless, some typical features of the results are seen even for small U . For instance, the resonance at finite U occurs for small value of $U/(2\pi t_x) \lesssim 1$ in the case of $t_y/t_x = 0.78$ as shown in Fig. 15 (a). Therefore we believe that the qualitative features of the results, such as the relation between the resonance and the eigenvalues of the effective Hamiltonian, hold also for large U . The perturbation approach gives us a correct, in principle, description of the conductance and the total charge displacement with respect to the local Fermi-liquid ground state.

§4. Summary

We have studied the conductance through small interacting systems connected to multi-mode leads based on a local Fermi-liquid approach. At $T = 0$, the conductance and the total charge displacement are determined by the value of the Green's function at the Fermi energy. Since the excitations at the Fermi energy do not decay at $T = 0$, there exists the one-particle Hamiltonian which reproduces these two quantities exactly. We have applied this formulation to a two-dimensional Hubbard model of finite size in the electron-hole symmetric case. We have calculated all the matrix elements of the order U^2 self-energy and determine the parameters of the effective Hamiltonian up to terms of order U^2 . Specifically, we have examined two types of the noninteracting leads: I) semi-infinite tight-binding leads, and II) leads of a constant density of states. The results are similar, qualitatively, in both types of the leads. The conductance shows maximums in the U dependence for some ranges of t_y/t_x , where t_x and t_y are the hopping matrix element in the x - and y -directions, respectively. This means that there exists parameter regions, where the total conductance increases with U , even in the half-filled case. By decomposing the total conductance into the sum of the contributions of the subbands, it is clarified that the peaks of the conductance are caused by the resonance occurring in some group of the subbands which have the similar symmetric properties. The phase shift of the subbands obtained from the Friedel sum rule shows a typical changes when the resonance occurs. The resonance generally does not occur simultaneously in different groups of the subbands, and the subbands of off-resonance behave monotonically. Therefore the maximum in the U dependence of the total conductance is expected only for the mesoscopic systems in which the number of the conducting modes is small enough and the contributions of the subbands of on-resonance are comparable to the those of the remaining subbands.

The perturbation approach examined in this work can be applied to interacting electrons in disordered systems. Especially, the analysis of the eigen values of the effective Hamiltonian, which is used in the present study to investigate the behaviors of the resonance, may be combined with

the Thouless-number²⁶⁾ and finite-size scaling²⁷⁾ methods. The application along this line seems to be interesting in relation to the metal-insulator transition observed in two-dimensional systems.²⁸⁾ Furthermore, extensions to the finite temperatures²⁹⁾ and nonequilibrium situations³⁰⁾ are left for future studies.

Acknowledgements

We would like to thank K. Murata, K. Tanigaki, and S. Nonoyama for valuable discussions. Numerical computation was partly performed at computation center of Nagoya University and at Yukawa Institute Computer Facility. This work was supported by the Grant-in-Aid for Scientific Research from the Ministry of Education, Science and Culture, Japan.

Appendix A: Conductance

In this appendix, we provide the derivation of the dc conductance in the multi-mode case eq. (2.9) by generalizing the derivation given in the single-mode case.¹⁶⁾ The current operator corresponding to the mixing term eq. (2.6) is given by

$$J_L = i e \sum_{m=1}^{M_L} \sum_{\sigma} v_{L,m} \left(c_{\mathcal{I}m\sigma}^{\dagger} c_{\mathcal{L}m\sigma} - c_{\mathcal{L}m\sigma}^{\dagger} c_{\mathcal{I}m\sigma} \right), \quad (\text{A}\cdot 1)$$

$$J_R = i e \sum_{m=1}^{M_R} \sum_{\sigma} v_{R,m} \left(c_{\mathcal{R}m\sigma}^{\dagger} c_{\mathcal{N}m\sigma} - c_{\mathcal{N}m\sigma}^{\dagger} c_{\mathcal{R}m\sigma} \right). \quad (\text{A}\cdot 2)$$

Here J_L is the total current flowing into the sample from the left lead, and J_R is the current flowing out to the right lead from the sample. These currents and the total charge in the sample $\rho_C = e \sum_{j \in C, \sigma} c_{j\sigma}^{\dagger} c_{j\sigma}$ satisfy the equation of continuity $\partial \rho_C / \partial t + J_R - J_L = 0$. In the linear response theory, the dc conductance is given by

$$g = \lim_{\omega \rightarrow 0} \frac{K_{\alpha\alpha'}^+(\omega) - K_{\alpha\alpha'}^+(0)}{i\omega}, \quad (\text{A}\cdot 3)$$

$$K_{\alpha\alpha'}(i\nu_l) = \int_0^{\beta} d\tau \langle T_{\tau} J_{\alpha}(\tau) J_{\alpha'}(0) \rangle e^{i\nu_l \tau}, \quad (\text{A}\cdot 4)$$

where $\alpha, \alpha' = L, R$, and $K_{\alpha\alpha'}^+(\omega)$ is the retarded function which is obtained from the Matsubara function $K_{\alpha\alpha'}(i\nu_l)$ by the analytic continuation $i\nu_l \rightarrow \omega + i0^+$. The dc conductance eq. (A.3) corresponds to the ω -linear imaginary part of $K_{\alpha\alpha'}^+(\omega)$, and it is independent of α and α' owing to the current conservation.^{31,32)} Moreover, $K_{\alpha'\alpha}(z) = K_{\alpha\alpha'}(z)$ because of the time reversal symmetry, and thus the imaginary part of $K_{\alpha\alpha'}^+(\omega)$ corresponds to the discontinuity of $K_{\alpha\alpha'}(z)$ along the real axis in the complex z -plane. Therefore, the dc conductance is equal to the coefficient of the $\nu \operatorname{sgn} \nu$ term of $K_{\alpha\alpha'}(i\nu)$,³⁵⁾ where $\operatorname{sgn} \nu$ is the sign function. In what follows, we extract this singular term from $K_{\alpha\alpha'}(i\nu)$ taking the current operators to be $\alpha = R$ and $\alpha' = L$.

At $T = 0$, $K_{RL}(i\nu)$ is written, treating the Matsubara frequencies to be continuous variables, as [see also Fig. 1]

$$K_{\text{RL}}(i\nu) = K_{\text{RL}}^{(a)}(i\nu) + K_{\text{RL}}^{(b)}(i\nu), \quad (\text{A}\cdot 5)$$

$$K_{\text{RL}}^{(a)}(i\nu) = e^2 \sum_{\sigma} \int_{-\infty}^{+\infty} \frac{d\varepsilon}{2\pi} \times \text{Tr} \left[\mathbf{v}_{\text{R}} \mathbf{G}_{\mathcal{RL}}(i\varepsilon + i\nu) \mathbf{v}_{\text{L}} \mathbf{G}_{\mathcal{LN}}(i\varepsilon) + \mathbf{v}_{\text{R}} \mathbf{G}_{\mathcal{NI}}(i\varepsilon + i\nu) \mathbf{v}_{\text{L}} \mathbf{G}_{\mathcal{LR}}(i\varepsilon) - \mathbf{v}_{\text{R}} \mathbf{G}_{\mathcal{RI}}(i\varepsilon + i\nu) \mathbf{v}_{\text{L}} \mathbf{G}_{\mathcal{LN}}(i\varepsilon) - \mathbf{v}_{\text{R}} \mathbf{G}_{\mathcal{NL}}(i\varepsilon + i\nu) \mathbf{v}_{\text{L}} \mathbf{G}_{\mathcal{IR}}(i\varepsilon) \right], \quad (\text{A}\cdot 6)$$

$$K_{\text{RL}}^{(b)}(i\nu) = e^2 \sum_{\sigma\sigma'} \sum_{\{j\} \in \text{C}} \int_{-\infty}^{+\infty} \frac{d\varepsilon d\varepsilon'}{(2\pi)^2} \Gamma_{\sigma\sigma'; \sigma'\sigma}^{j_1 j_2; j_3 j_4}(i\varepsilon + i\nu, i\varepsilon' + i\nu; i\varepsilon', i\varepsilon) \times \left\{ \mathbf{G}_{\text{CL}}(i\varepsilon + i\nu) \mathbf{v}_{\text{L}} \mathbf{G}_{\text{IC}}(i\varepsilon) - \mathbf{G}_{\text{CI}}(i\varepsilon + i\nu) \mathbf{v}_{\text{L}} \mathbf{G}_{\text{LC}}(i\varepsilon) \right\}_{j_1 j_4} \times \left\{ \mathbf{G}_{\text{CN}}(i\varepsilon') \mathbf{v}_{\text{R}} \mathbf{G}_{\text{RC}}(i\varepsilon' + i\nu) - \mathbf{G}_{\text{CR}}(i\varepsilon') \mathbf{v}_{\text{R}} \mathbf{G}_{\text{NC}}(i\varepsilon' + i\nu) \right\}_{j_3 j_2}. \quad (\text{A}\cdot 7)$$

Here \mathbf{v}_{L} and \mathbf{v}_{R} are diagonal matrices corresponding to $v_{\text{L},m}$ and $v_{\text{R},m}$, respectively. The subscript C denotes a set consisting of N_{C} sites in the central region. $\mathbf{G}_{\text{CL}}(z)$ is a $N_{\text{C}} \times M_{\text{L}}$ matrix, and the (j, m) element is given by $G_{j, \mathcal{L}m}(z)$ with $j \in \text{C}$. Also, $\mathbf{G}_{\text{RC}}(z)$ is a $M_{\text{R}} \times N_{\text{C}}$ matrix, and the (m, j) element is given by $G_{\mathcal{R}m, j}(z)$ with $j \in \text{C}$. The matrix Green's functions in eqs. (A.6) and (A.7) are defined in this way. $\Gamma_{\sigma\sigma'; \sigma'\sigma}^{j_1 j_2; j_3 j_4}(i\varepsilon_1, i\varepsilon_2; i\varepsilon_3, i\varepsilon_4)$ is the vertex corrections due to the inter-electron interaction, and illustrated in Fig. 18. Since we are considering the interaction which is switched on only in the central region, the Green's function satisfies following relations at the interfaces;

$$\begin{cases} \mathbf{G}_{\mathcal{R}\gamma}(z) = -\mathbf{F}_{\text{R}}(z) \mathbf{v}_{\text{R}} \mathbf{G}_{\mathcal{N}\gamma}(z) & \text{for } \gamma = \mathcal{L}, \mathcal{I}, \text{C}, \mathcal{N} \\ \mathbf{G}_{\gamma\mathcal{L}}(z) = -\mathbf{G}_{\gamma\mathcal{I}}(z) \mathbf{v}_{\text{L}} \mathbf{F}_{\text{L}}(z) & \text{for } \gamma = \mathcal{I}, \text{C}, \mathcal{N}, \mathcal{R} \end{cases}. \quad (\text{A}\cdot 8)$$

Using these relations, eqs. (A.6) and (A.7) are rewritten as

$$K_{\text{RL}}^{(a)}(i\nu) = e^2 \sum_{\sigma} \int_{-\infty}^{+\infty} \frac{d\varepsilon}{2\pi} \text{Tr} \left[\mathbf{v}_{\text{R}} [\mathbf{F}_{\text{R}}(i\varepsilon + i\nu) - \mathbf{F}_{\text{R}}(i\varepsilon)] \mathbf{v}_{\text{R}} \mathbf{G}_{\mathcal{NI}}(i\varepsilon + i\nu) \times \mathbf{v}_{\text{L}} [\mathbf{F}_{\text{L}}(i\varepsilon + i\nu) - \mathbf{F}_{\text{L}}(i\varepsilon)] \mathbf{v}_{\text{L}} \mathbf{G}_{\mathcal{LN}}(i\varepsilon) \right], \quad (\text{A}\cdot 9)$$

$$K_{\text{RL}}^{(b)}(i\nu) = e^2 \sum_{\sigma\sigma'} \sum_{\{j\} \in \text{C}} \int_{-\infty}^{+\infty} \frac{d\varepsilon d\varepsilon'}{(2\pi)^2} \Gamma_{\sigma\sigma'; \sigma'\sigma}^{j_1 j_2; j_3 j_4}(i\varepsilon + i\nu, i\varepsilon' + i\nu; i\varepsilon', i\varepsilon) \times \left\{ \mathbf{G}_{\text{CI}}(i\varepsilon + i\nu) \mathbf{v}_{\text{L}} [\mathbf{F}_{\text{L}}(i\varepsilon + i\nu) - \mathbf{F}_{\text{L}}(i\varepsilon)] \mathbf{v}_{\text{L}} \mathbf{G}_{\text{IC}}(i\varepsilon) \right\}_{j_1 j_4}$$

$$\times \left\{ \mathbf{G}_{\mathcal{CN}}(i\varepsilon') \mathbf{v}_R [\mathbf{F}_R(i\varepsilon' + i\nu) - \mathbf{F}_R(i\varepsilon')] \mathbf{v}_R \mathbf{G}_{\mathcal{NC}}(i\varepsilon' + i\nu) \right\}_{j_3 j_2}. \quad (\text{A}\cdot 10)$$

We can now extract the singular $\nu \operatorname{sgn} \nu$ term of $K_{\text{RL}}(i\nu)$ using eqs. (A·9) and (A·10), as in the case of the single Anderson impurity.^{35,36)} It can be shown that there is no singular $\nu \operatorname{sgn} \nu$ term in $K_{\text{RL}}^{(b)}(i\nu)$ due the two factors $[\mathbf{F}_L(i\varepsilon + i\nu) - \mathbf{F}_L(i\varepsilon)]$ and $[\mathbf{F}_R(i\varepsilon' + i\nu) - \mathbf{F}_R(i\varepsilon')]$ which have different frequencies. Thus, the $\nu \operatorname{sgn} \nu$ term comes only from $K_{\text{RL}}^{(a)}(i\nu)$. It can be obtained from eq. (A·9) and yields eq. (2.9).

Appendix B: Friedel sum rule

We provide here the outline of the derivation of the Friedel sum rule in the single-mode case eq. (B·7) following Langer and Ambegaokar.³³⁾ The Green's function in the left lead $ij \in \text{L}$ is written as

$$G_{ij}^+(\omega) = F_{ij}^L(\omega) + F_{i0}^L(\omega) v_L G_{11}^+(\omega) v_L F_{0j}^L(\omega), \quad (\text{B}\cdot 1)$$

$$F_{ij}^L(\omega) = \sum_n \frac{\phi_{n,\text{L}}(i) \phi_{n,\text{L}}^*(j)}{\omega - \epsilon_{n,\text{L}} + i0^+}. \quad (\text{B}\cdot 2)$$

Here $F_{ij}^L(\omega)$ is the retarded Green's function of the isolated lead, and $\epsilon_{n,\text{L}}$ and $\phi_{n,\text{L}}(i)$ are the eigenvalue and the corresponding eigenfunction of the one-particle Hamiltonian \mathcal{H}_L . Using the orthogonality relation $\sum_{i \in \text{L}} \phi_{n,\text{L}}(i) \phi_{n',\text{L}}^*(i) = \delta_{nn'}$, we obtain

$$\sum_{i \in \text{L}} [G_{ii}^+ - F_{ii}^L] = -\frac{\partial F_{00}^L}{\partial \omega} v_L G_{11}^+ v_L. \quad (\text{B}\cdot 3)$$

Here $F_{00}^L \equiv F_L^+$, which is the Green's function at the interface. Using eq. (B·3) and the corresponding relation for the right lead, the displacement of the total charge defined by eq. (2.10) is written, at $T = 0$, as

$$\begin{aligned} \Delta N_{\text{tot}} &= -\frac{2}{\pi} \operatorname{Im} \int_{-\infty}^0 d\omega \left(\sum_{i \in \text{C}} G_{ii}^+ + \sum_{i \in \text{L}} [G_{ii}^+ - F_{ii}^L] + \sum_{i \in \text{R}} [G_{ii}^+ - F_{ii}^R] \right) \\ &= -\frac{2}{\pi} \operatorname{Im} \int_{-\infty}^0 d\omega \operatorname{Tr} \left[\mathbf{g}^+ - \mathbf{g}^+ \frac{\partial \mathbf{V}_{\text{mix}}^+}{\partial \omega} \right] \\ &= -\frac{2}{\pi} \operatorname{Im} \int_{-\infty}^0 d\omega \left(\frac{\partial}{\partial \omega} \operatorname{Tr} [\log \{\mathbf{g}^+\}^{-1}] + \operatorname{Tr} \left[\mathbf{g}^+ \frac{\partial \mathbf{\Sigma}^+}{\partial \omega} \right] \right). \end{aligned} \quad (\text{B}\cdot 4)$$

Here we have used a matrix notation as that was used in the text eqs. (3.1)-(3.4) for the multi-mode case: the Green's function in the central region is denoted by $\mathbf{g}(z) = \{G_{ij}(z)\}$ with $ij \in \text{C}$ and

the Dyson equation is given by $\{\mathcal{G}(z)\}^{-1} = z \mathbf{1} - \mathcal{H}_C^0 - \mathcal{V}_{\text{mix}}(z) - \Sigma(z)$, where $\mathcal{H}_C^0 = \{-t_{ij}^C - \mu \delta_{ij}\}$, and $\mathcal{V}_{\text{mix}}(z)$ and $\Sigma(z)$ are the single-mode version of eqs. (3.3) and (3.4), respectively.

It has been shown that the contribution of the second term in the third line of eq. (B.4) vanishes.^{37,38)} Thus, eq. (B.4) can be rewritten as

$$\Delta N_{\text{tot}} = \frac{1}{\pi i} \log \left[\det \{\mathcal{G}^-(0)\}^{-1} / \det \{\mathcal{G}^+(0)\}^{-1} \right] \quad (\text{B}\cdot 5)$$

$$= \frac{1}{\pi i} \log \det \left[\mathbf{1} + 2i \text{Im} \left\{ \mathcal{V}_{\text{mix}}^+(0) \right\} \mathcal{G}^+(0) \right]. \quad (\text{B}\cdot 6)$$

For obtaining eq. (B.6), we have used the Fermi-liquid property $\text{Im}\Sigma^+(0)$. The matrix \mathcal{V}_{mix} has only two non-zero elements as eq. (3.3). Therefore, the determinant in eq. (B.6) can be written in terms of a 2×2 matrix as

$$\Delta N_{\text{tot}} = \frac{1}{\pi i} \log[\det \mathbf{S}], \quad (\text{B}\cdot 7)$$

$$\mathbf{S} = \begin{bmatrix} 1 & 0 \\ 0 & 1 \end{bmatrix} - 2i \begin{bmatrix} \Gamma_L(0) & 0 \\ 0 & \Gamma_R(0) \end{bmatrix} \begin{bmatrix} G_{11}^+(0) & G_{1N}^+(0) \\ G_{N1}^+(0) & G_{NN}^+(0) \end{bmatrix}. \quad (\text{B}\cdot 8)$$

-
- [1] See, for instance, T. Ishiguro, K. Yamaji and G. Saito: *Organic Superconductors Second Edition*, (Springer-Verlag, Berlin, 1998).
- [2] T. K. Ng and P. A. Lee: Phys. Rev. Lett. **61** (1988) 1768.
- [3] L. I. Glazman and M. E. Raikh: Pis'ma Zh. Eksp. Teor. Fiz. **47** (1988) 378, [JETP Lett. **47** 452 (1988)].
- [4] A. Kawabata: J. Phys. Soc. Jpn. **60** (1991) 3222.
- [5] Y. Meir, N. S. Wingreen and P. A. Lee: Phys. Rev. Lett. **66** (1991) 3048; *ibid.* **70** (1993) 2601.
- [6] S. Hershfield, J. H. Davies and J. W. Wilkins: Phys. Rev. B **46** (1992) 7046.
- [7] D. C. Ralph and R. A. Buhrman: Phys. Rev. Lett. **72** (1994) 3401.
- [8] D. Goldharber-Gordon, H. Shtrikman, D. Mahalu, D. Abusch-Magder, U. Meirav and M. A. Kastner: Nature **391** (1998) 156.
- [9] S. M. Cronenwett, T. H. Oosterkamp and L. P. Kouwenhoven: Science **281** (1998) 540.
- [10] T. H. Oosterkamp, T. Fujisawa, W.G. van der Wiel, K. Ishibashi, R. V. Hijman, S. Tarucha and L. P. Kouwenhoven: Nature **395** (1998) 873.
- [11] Y. Tokura, D. G. Austing and S. Tarucha: J. Phys.: Condens. Matter **56** (1999) 6023.
- [12] W. Izumida, O. Sakai and Y. Shimizu: J. Phys. Soc. Jpn. **66** (1997) 717; *ibid.* **67** (1998) 2444.
- [13] W. Izumida and O. Sakai: Phys. Rev. B **62** (2000) 10260; W. Izumida, O. Sakai and S. Suzuki: J. Phys. Soc. Jpn. **70** (2001) 1045.
- [14] O. Sakai, S. Suzuki, W. Izumida and A. Oguri: J. Phys. Soc. Jpn. **68** (1999) 1640.
- [15] A. Oguri, H. Ishii and T. Saso: Phys. Rev. B **51** (1995) 4715.
- [16] A. Oguri: Phys. Rev. B **56** (1997) 13422 [Errata: **58** (1998) 1690].
- [17] A. Oguri: Phys. Rev. B **59** (1999) 12240.
- [18] A. Oguri: Phys. Rev. B **63** (2001) 115305 [Errata: **63** (2001) 249901].
- [19] A. Yeyati, A. Martín-Rodero and F. Flores: Phys. Rev. Lett. **71** (1993) 2991.

- [20] T. Mii and K. Makoshi: Jpn. J. Appl. Phys. **35** (1996) 3706.
- [21] O. Takagi and T. Saso: J. Phys. Soc. Jpn. **68** (1999) 1997.
- [22] P. L. Pernas, F. Flores and E. V. Anda: J. Phys.: Condens. Matter **4** (1992) 5309.
- [23] Y. Kawahito, H. Kasai, H. Nakanishi and A. Okiji: J. Appl. Phys. **85** (1999) 947.
- [24] N. D. Lang and Ph. Avouris: Phys. Rev. Lett. **84** (1999) 358.
- [25] P. W. Anderson: Phys. Rev. **124** (1961) 41.
- [26] D. C. Licciardello and D. J. Thouless: J. Phys. C **8** (1975) 4157.
- [27] A. MacKinnon and B. Kramer: Z. Phys. B **53** (1983) 1.
- [28] S. V. Kravchenko, G. V. Kravchenko, J. E. Furneaux, V. M. Pudalov and M. D'Iorio: Phys. Rev. B **50** (1994) 8039.
- [29] A. Oguri: J. Phys. Soc. Jpn. **70**, (2001) 2666.
- [30] A. Oguri: Phys. Rev. B **64**, (2001) 153305.
- [31] D. S. Fisher and P. A. Lee: Phys. Rev. B **23** (1981) 6851.
- [32] P. A. Lee and D. S. Fisher: Phys. Rev. Lett. **47** (1981) 882.
- [33] J. S. Langer and V. Ambegaokar: Phys. Rev. **121** (1961) 1090.
- [34] D. C. Langreth: Phys. Rev. **150** (1966) 516.
- [35] H. Shiba: Prog. Theor. Phys. **54** (1975) 967.
- [36] A. Oguri: Phys. Rev. B **52** (1995) 16727.
- [37] J. M. Luttinger and J. C. Ward: Phys. Rev. **118** (1960) 1417.
- [38] J. M. Luttinger: Phys. Rev. **119** (1960) 1153.

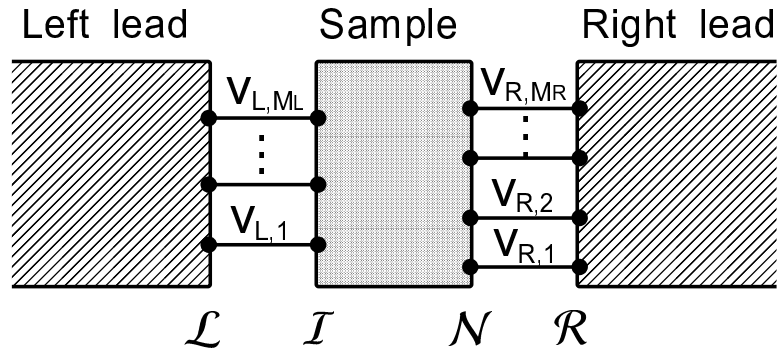


Fig. 1. Schematic picture of the system.

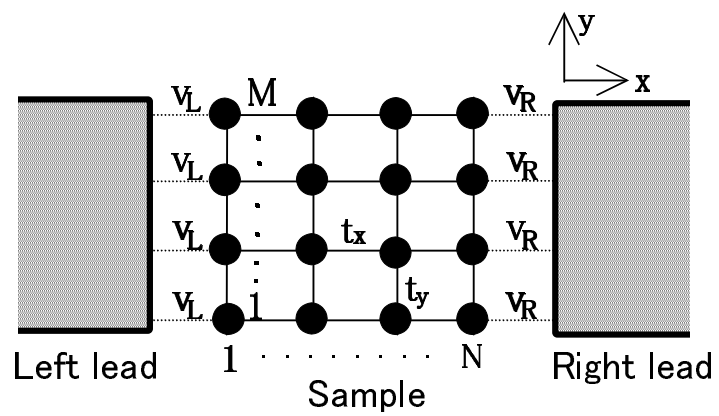


Fig. 2. Schematic picture of a 2D Hubbard model: (\bullet) interacting sites.

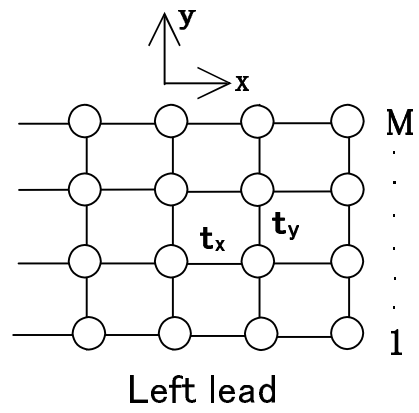


Fig. 3. Schematic picture of the type I lead.

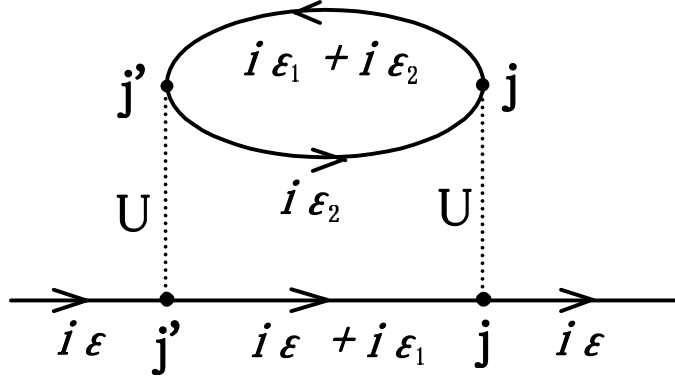


Fig. 4. The order U^2 self-energy $\Sigma_{jj'}(i\varepsilon)$.

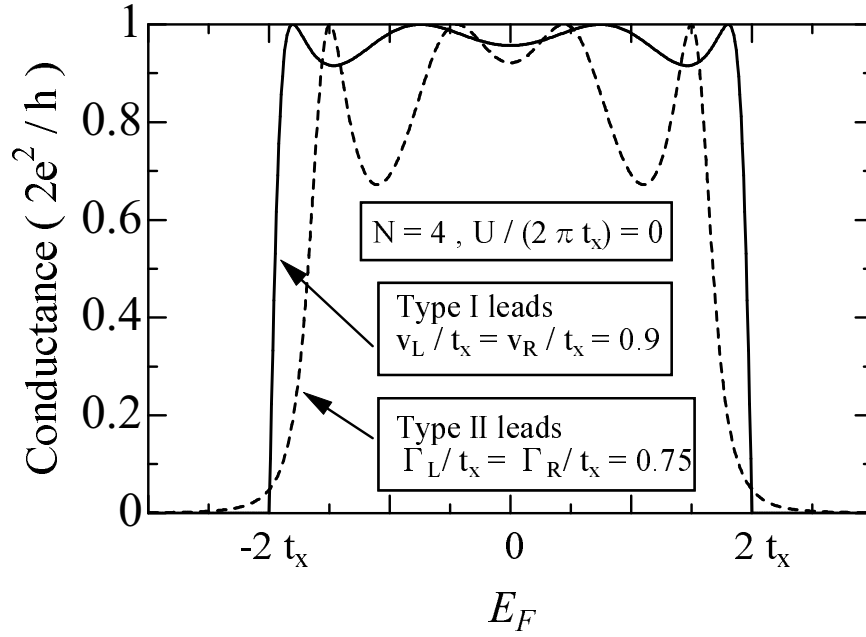


Fig. 5. Conductance vs. E_F for noninteracting electrons on the one-dimensional chain of the size $N = 4$ connected to the leads; (solid line) type I leads and (dashed line) type II leads.

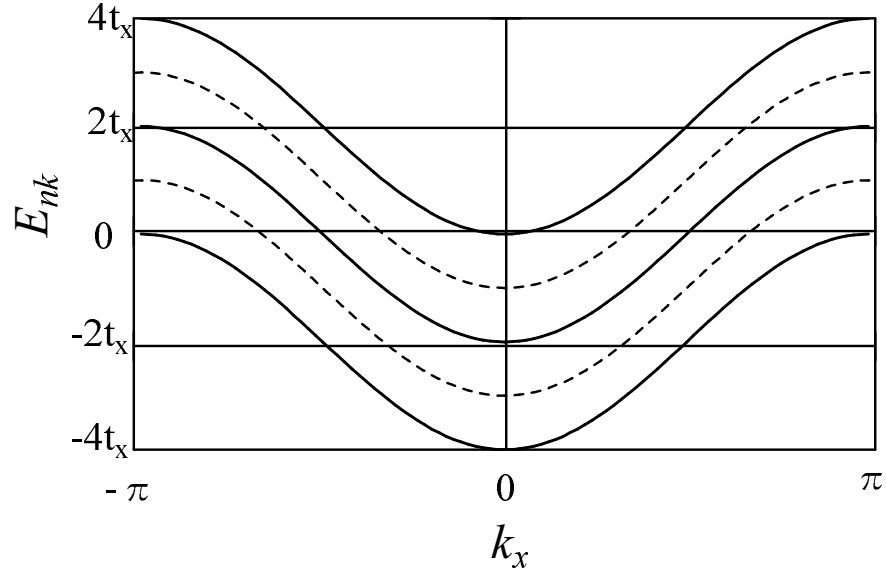


Fig. 6. Subband structure of the type I lead of the width $M = 4$, where (solid line) $t_y/t_x = 1.0$ and (dashed line) $t_y/t_x = 0.5$.

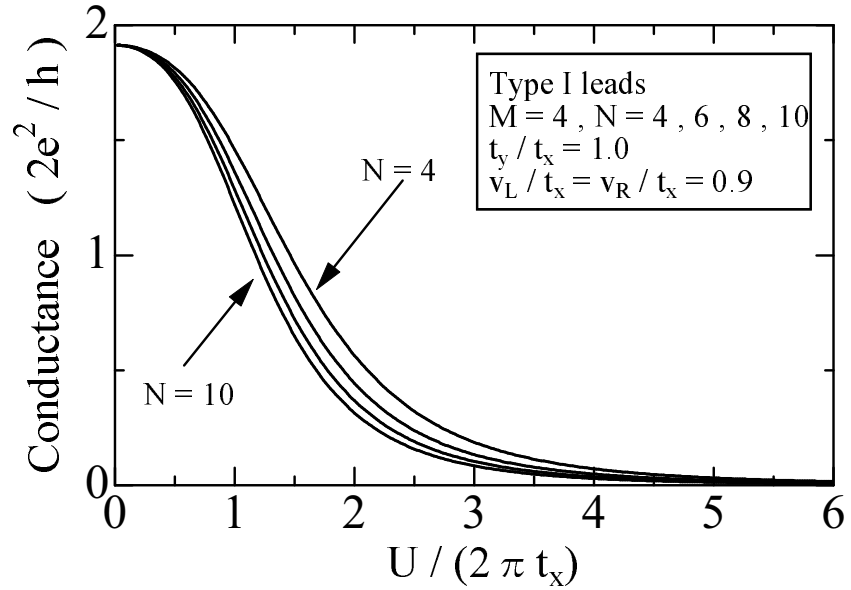


Fig. 7. Conductance vs. U in the isotropic case of $t_y/t_x = 1.0$. The size of the interacting region is chosen to be $M = 4$ and $N = 4, 6, 8, 10$. Type I leads.

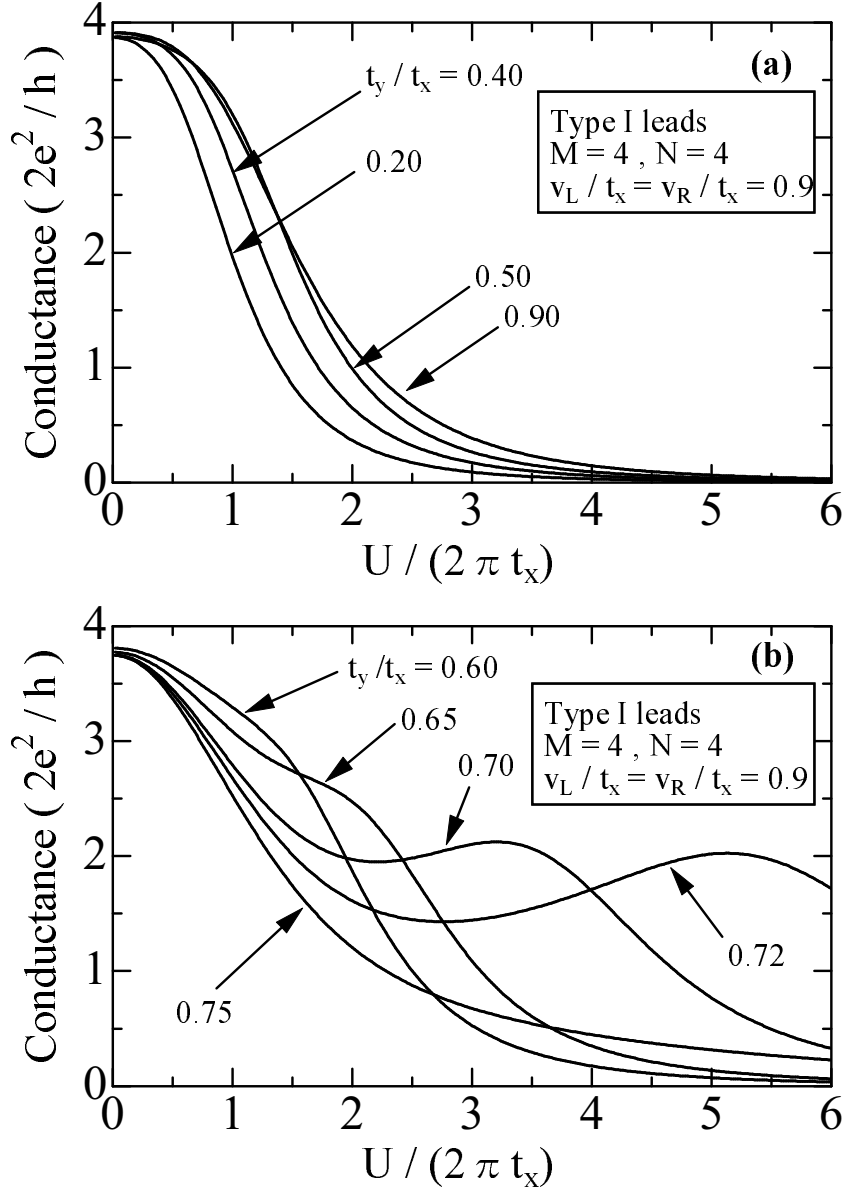


Fig. 8. Conductance vs. U in the anisotropic case $t_y/t_x < 1.0$. The size of the interacting region is chosen to be $M = 4$ and $N = 4$. Type I leads.

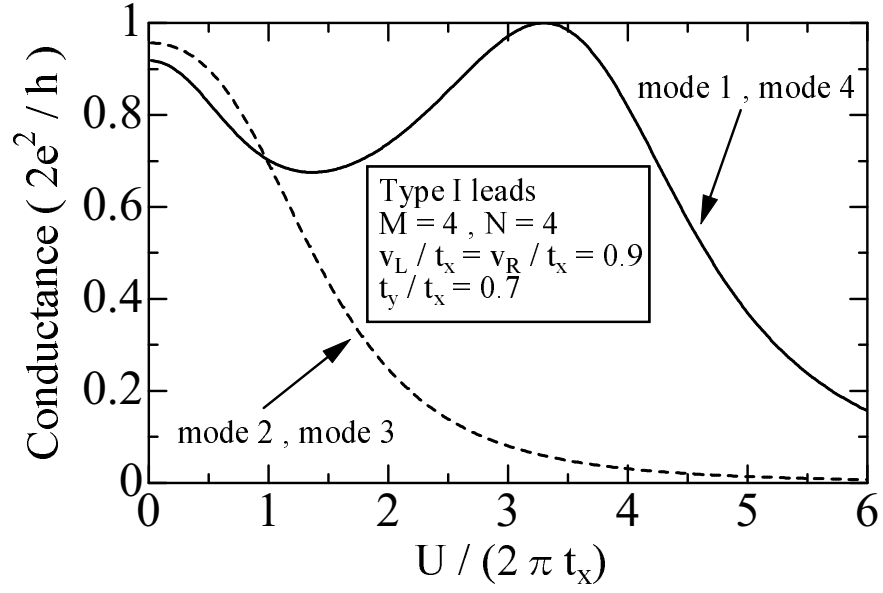


Fig. 9. Conductance of each subband, where $M = 4$, $N = 4$, and $t_y/t_x = 0.7$. Type I leads.

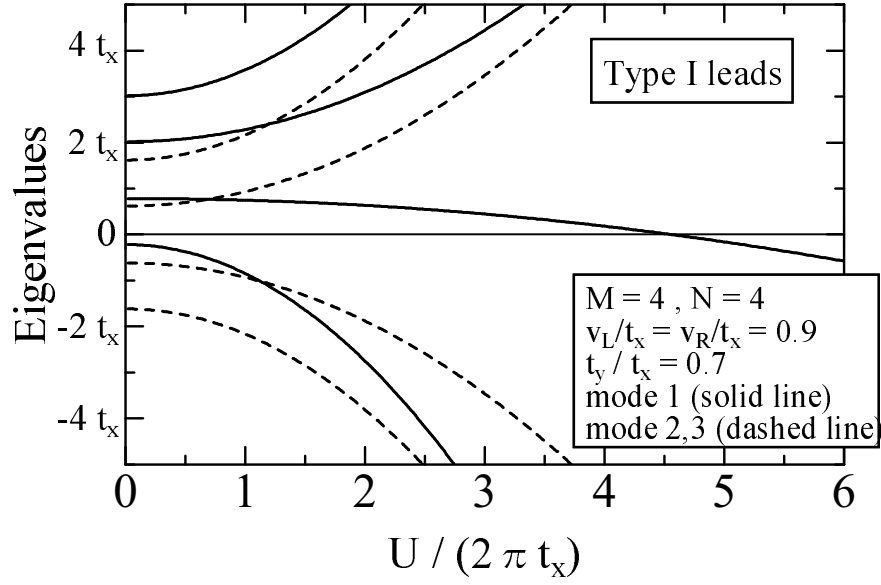


Fig. 10. Eigenvalues of $\tilde{\mathcal{H}}_C^{(n)}$ for $n = 1$ (solid line) and $n = 2, 3$ (dashed line), where $M = 4$, $N = 4$, and $t_y/t_x = 0.7$. The origin of the energy is set to be $E_F = 0$. Type I leads.

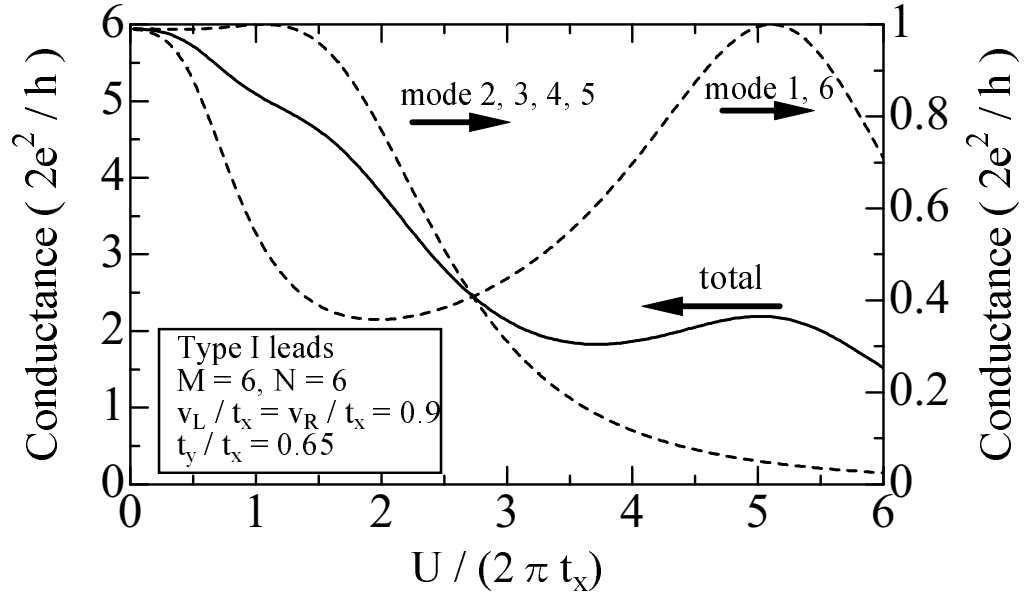


Fig. 11. Conductance vs. U for the system of the size $M = 6$ and $N = 6$: (solid line) total conductance and (dashed line) contributions of each mode for $t_y/t_x = 0.65$. Type I leads.

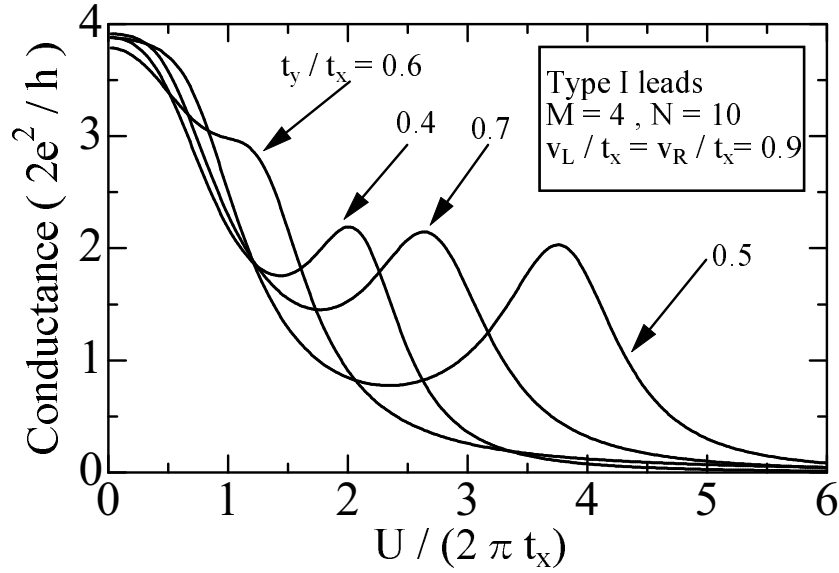


Fig. 12. Conductance vs. U for the system of the size $M = 4$ and $N = 10$, where $t_y/t_x = 0.4, 0.5, 0.6$, and 0.7 . Type I leads.

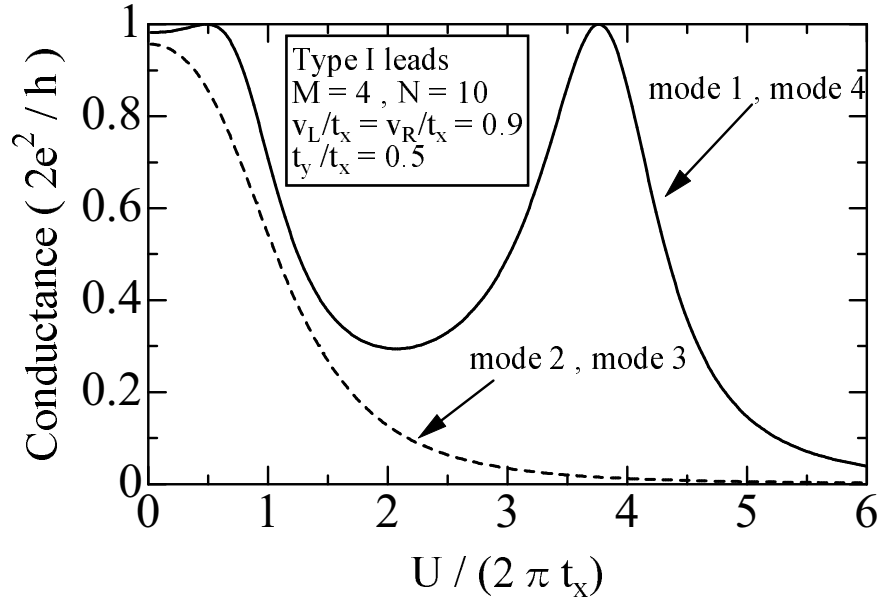


Fig. 13. Conductance of each subband for the system of the size $M = 4$ and $N = 10$, where $t_y/t_x = 0.5$. Type I lead.

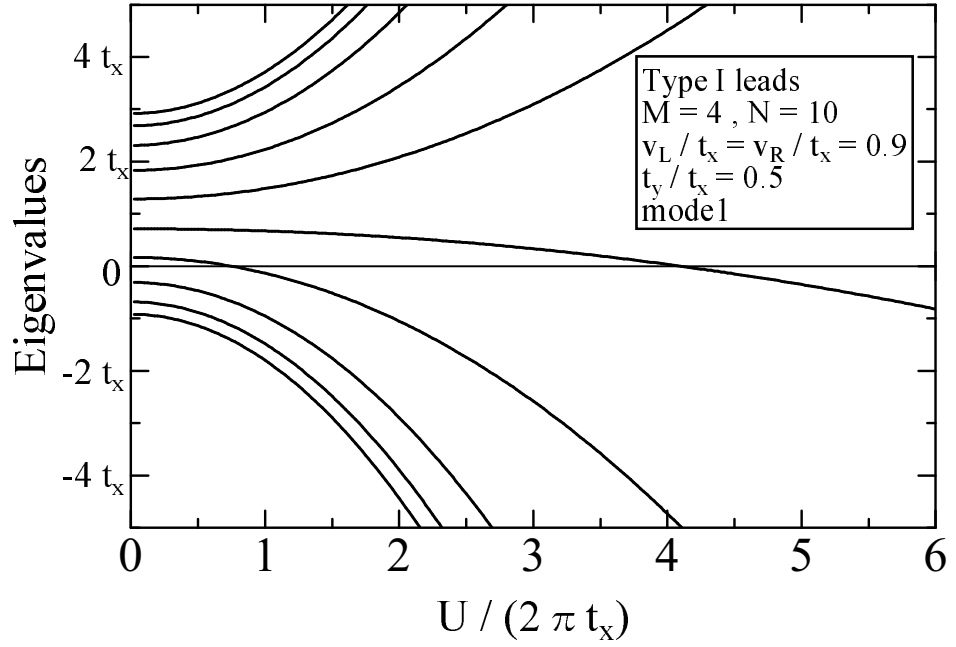


Fig. 14. Eigenvalues of $\tilde{\mathcal{H}}_C^{(n)}$ for $n = 1$, where $M = 4$, $N = 10$, and $t_y/t_x = 0.5$. The origin of the energy is set to be $E_F = 0$. Type I leads.

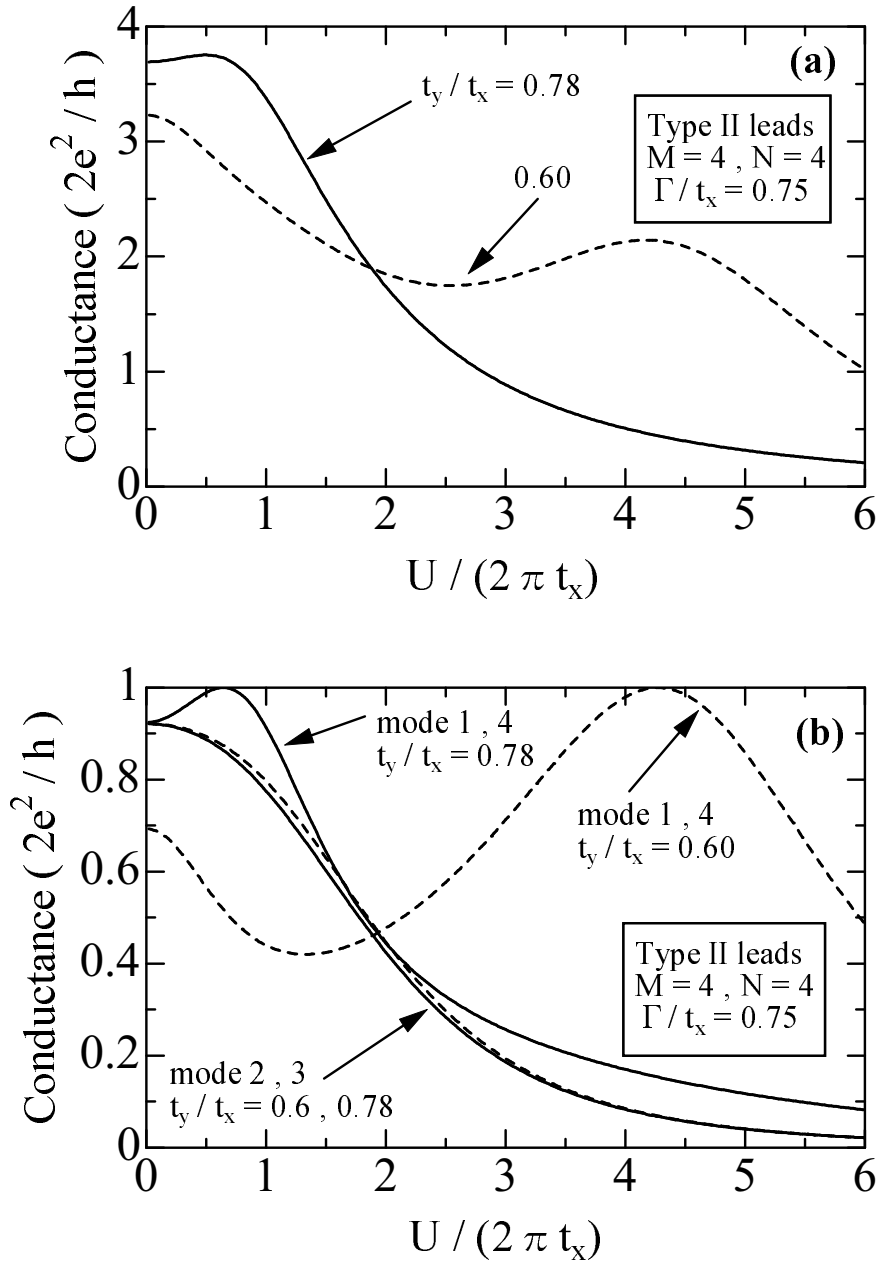


Fig. 15. Conductance vs. U for the system of $M = 4$ and $N = 4$ in the case of the type II leads: (a) total conductance, and (b) contributions of each mode. The hopping matrix element is taken to be (dashed line) $t_y/t_x = 0.6$, and (solid line) 0.78 .

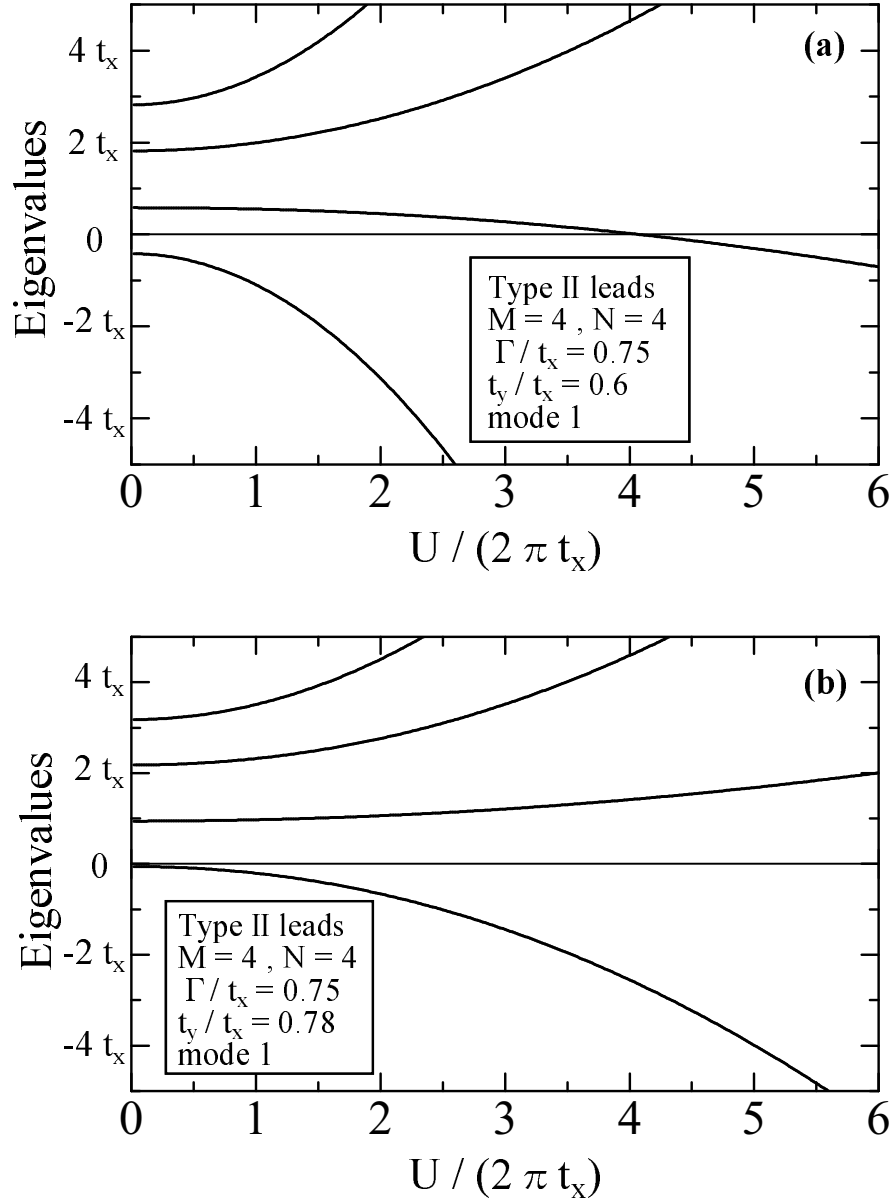


Fig. 16. Eigenvalues of $\tilde{\mathcal{H}}_C^{(n)}$ for $n = 1$, where $M = 4$ and $N = 4$. The hopping matrix element is taken to be (a) $t_y/t_x = 0.6$ and (b) 0.78 . The origin of the energy is set to be $E_F = 0$. Type II leads.

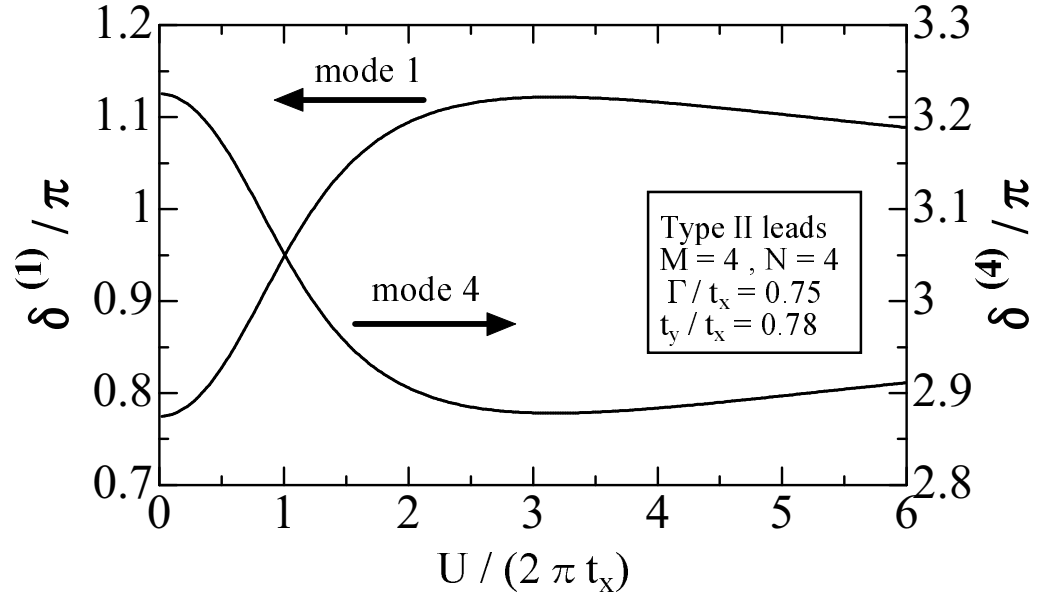


Fig. 17. Phase shift $\delta^{(n)}/\pi$ vs. U for $n = 1$ and $n = 4$, where $M = 4$, $N = 4$, and $t_y/t_x = 0.78$. Type II leads.

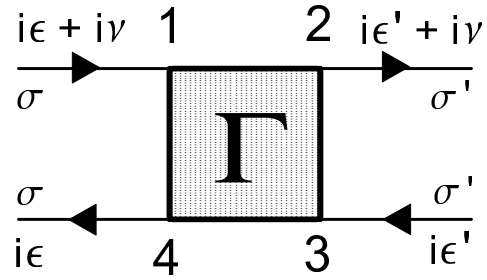


Fig. 18. The vertex function $\Gamma_{\sigma\sigma';\sigma'\sigma}^{j_1j_2;j_3j_4}(i\varepsilon + i\nu, i\varepsilon' + i\nu; i\varepsilon', i\varepsilon)$.